Presented at the 5th National Conference on Synchrotron Radiation Instrumentation, Madison, Wisconsin, June 21-25, 1987

CCD SENSORS IN SYNCHROTRON X-RAY DETECTORS*

M. G. Strauss, I. Naday+, I. S. Sherman, M. R. Kraimer
E. M. Westbrook and N. J. Zaluzec

Argonne National Laboratory
Argonne, Illinois 60439, USA

ABSTRACT

The intense photon flux from advanced synchrotron light sources, such as the 7-Gev synchrotron being designed at Argonne, require integrating-type detectors. Charge-coupled devices (CCDs) are well suited as synchrotron x-ray detectors. When irradiated indirectly via a phosphor followed by reducing optics, diffraction patterns of 100 cm^2 can be imaged on a 2 cm^2 CCD. With a conversion efficiency of ~1 CCD electron/x-ray photon, a peak saturation capacity of $>10^6$ x rays can be obtained. A programmable CCD controller operating at a clock frequency of 20 MHz has been developed. The readout rate is $5x10^6$ pixels/s and the shift rate in the parallel registers is 10^6 lines/s. The test detector was evaluated in two experiments. In protein crystallography diffraction patterns have been obtained from a lysozyme crystal using a conventional rotating anode x-ray generator. Based on these results we expect to obtain at a synchrotron diffraction images at the rate of ~1 frame/s or a complete 3-dimensional data set from a single crystal in ~2 min.

---

* Work supported by the U. S. Department of Energy under Contract W-31-109-Eng-38.

+ Present address: Central Research Institute for Physics, P. O. Box 49, H-1525 Budapest, Hungary

DISCLAIMER

In electron energy-loss spectroscopy (EELS), the CCD was used in a parallel detection mode which is similar to the mode array detectors are used in dispersive EXAFS. With a beam current corresponding to $3x10^9$ electrons/s on the detector, a series of 64 spectra were recorded on the CCD in a continuous sequence without interruption due to readout. The frame-to-frame pixel signal fluctuations had a $\bar{\sigma}$= 0.4% from which a DQE=0.4 was obtained, where the detector conversion efficiency was 2.6 CCD electrons/x-ray photon. These multiple frame series also showed the time-resolved modulation of the electron microscope optics by stray magnetic fields.

1. Introduction

The intense photon flux produced by synchrotron x-ray sources creates unprecedented opportunities in many areas of synchrotron radiation research. The extent to which these opportunities can be realized depends to a large degree on the availability of suitable detectors. The most important performance criterion of a detector for synchrotrons is its response to the x-ray input rate. Considering the output of the 7-GeV synchrotron being designed at Argonne,[1] the time-averaged flux on a detector could reach 10^{15} ph/s. With an orbit revolution time of 3.5 us and 50 bunches each having a duration of 50 ps, the instantaneous rate is 10^{18} ph/s. To count at this rate requires a detector with a pulse-pair resolution of 10^{-18}s which is ~10 orders of magnitude beyond the capability of a counting detector. It is this limitation which is the underlying rationale for the development of an integrating-type detector.

For the past three years we have been developing detectors

which incorporate a charge-coupled device (CCD). Our objective is to develop a basic detector system which could be configured to meet the requirements of diverse scientific applications particularly those in synchrotron radiation research such as macromolecular crystallography, EXAFS, and coronary angiography. X-ray detectors incorporating a CCD have been developed by Dalglish et al.[2] and Eikenberry et al.[3] but have not been used in experiments with synchrotron light sources. While CCDs have no limitations in their rate response, they have other performance limitations which will be discussed here.

In this paper we consider some of the CCD properties pertaining to detectors for synchrotron x rays. We then outline how we incorporate CCDs in a detector system and how we program the CCDs to meet a wide range of requirements in synchrotron radiation research. Finally, we present results from initial experiments using a prototype CCD-based detector system.

2. CCD Detector Design Considerations

A CCD sensor can be considered as an array of coupled photo-sensitive capacitors, where each capacitor constitutes a pixel in the array[4,5]. Light photons impinging on the CCD create electrons which are collected in a pixel well at the point of the photon incidence. A conceptual drawing of a frame-transfer CCD is shown in Fig. 1. Areas A and B are photo sensitive. Area A serves as the imaging area and area B, which is masked, serves as the image storage area. Each pixel has three electrodes, Ø1, Ø2, and Ø3 as shown in the enlarged section in Fig. 1. Charge transfer from pixel to pixel is carried out by sequentially

pulsing these electrodes. After an exposure, the image in area A is rapidly shifted by charge transfer, line by line, from area A to area B without readout and while the next exposure is taken in area A the image in area B is read out. Readout proceeds by shifting one line at a time from area B into the horizontal register. From the horizontal register the pixel charge is shifted out one at a time, amplified, digitized, and then stored in memory. Thus it is seen that readout from a CCD is a serial process which is relatively slow compared with a parallel readout detector.

The readout rate does not always limit the framing rate. When the imaging area is only a fraction of the CCD area and the storage area is increased accordingly, one can expose a series of frames in rapid succession where after each exposure the frame is shifted into the storage area, but is not read out. Thus, a sequence of frames can be acquired at a rate which is not limited by the readout rate. This mode of operation is of particular value for acquiring time-resolved 1-dimensional data as in spectroscopy.

Area CCDs can have as many as several million pixels and therefore for most synchrotron applications they would have adequate spatial resolution. The pixel of a typical CCD has a lateral dimension of 10-30 μm (Fig. 1). The largest available CCD of 2048^2 pixels has an imaging area of 55x55 mm^2. A more common CCD of 512^2 pixels has an imaging area less than 15x15 mm^2. For applications such as coronary angiography and protein crystallography the CCD is smaller than the image of interest, whereas for topography it may be too large. Thus the image size

must be altered to match the CCD area[6].

The minimum useful signal from a CCD is determined by the dark current noise, the read noise, and the digitization noise. The dark current noise is that due to leakage current in the CCD pixels. The read noise is that produced in the analog chain which consists of the on-chip amplifier, video amplifier, and sample-and-hold circuits. The digitization noise is that produced in quantization by the ADC. The maximum signal is determined by the pixel well capacity. The ratio of the maximum signal to the total RMS noise determines the dynamic range of a CCD pixel. However, in scientific applications an information cell, e.g., a peak, is usually of interest rather than a single pixel. When a peak is contained in several pixels, the signals in these pixels add algebraically while the noise adds in quadrature. Thus, the dynamic range seen in the data would increase with the square root of the number of pixels in the peak. The statistical precision in the data is largely determined from the number of x rays in the peak which in turn is limited by the CCD well capacity which is generally governed by the pixel size.

3. CCD Detector Configuration

In order to overcome the limitations of CCD size and well capacity as well as for other reasons, e.g., radiation damage, the CCD is not exposed to the x rays directly, but is incorporated in a system comprised of a combination of components, which include fluorescent phosphor, optics, image sensor, analog-to-digital converter, and data processors and

stores. A diagram of the generic components and their function is shown in Fig. 2. X rays absorbed in the phosphor give rise to fluorescent light. The light image is demagnified (or magnified) and focused on the image sensor (CCD) by the optical system which includes a lens system and/or a fiberoptic taper and/or an image intensifier. Light photons impinging on the CCD create electrons which are collected in discrete pixels at the point of photon incidence. Thus, a 2-dimensional image is formed in the CCD where the intensity of each point is determined by the number of electrons in the pixel. At the end of the accumulation period, the CCD is read out thus producing video pulses. The pulses are digitized and temporarily stored in a fast buffer memory. When the CCD readout is completed, the next frame accumulation commences and the data previously stored in the buffer memory are transferred to the computer for permanent storage and display.

By using a large phosphor screen followed by reducing optics, one can record an image considerably larger than the CCD area. The phosphor should have a fast decay to permit time-resolved studies, high light output to offset the losses in the reducing optics, and a spatial resolution exceeding that of the CCD.

The statistical precision in the data is limited by the number of x rays recorded in a CCD pixel which is a strong function of the conversion efficiency. The conversion efficiency E determines the average electron yield in a pixel due to an incident x-ray photon on the phosphor. The conversion efficiency is therefore equal to the product of the fluorescent yield of the phosphor, the transmission efficiency of the optical

system, and the quantum efficiency of the CCD. Since the full-well electron capacity of a pixel is limited, the conversion efficiency also determines the maximum pixel capacity in terms of x-ray photons, and in turn, the maximum x-ray count in a peak or the peak saturation capacity. The higher the conversion efficiency the lower the maximum number of x rays that can be recorded in a pixel and consequently in a peak. In order to detect the maximum number of x rays in a given exposure time, the conversion efficiency is designed to be near unity[7]. If E is less than unity, only a fraction of the incident x-ray photons are recorded and a longer exposure time would be required to obtain peak saturation capacity. If E is greater than unity, the saturation capacity in terms of x rays is smaller and would, therefore, result in reduced statistical precision. This is the case when the the CCD is exposed to the x rays directly rather than indirectly as shown in Fig. 2.

While a system using indirect exposure provides for higher peak saturation capacity, it also introduces detection uncertainties not present in a direct exposure system. These additional uncertainties are due to statistical fluctuations in the light yield of the phosphor and the transfer efficiency of the reducing optics. The total uncertainty in the output signal will include the above mentioned fluctuations as well those in the CCD quantum efficiency and noise due to dark current, readout, and digitization. The figure of merit of detector precision is given by the detective quantum efficiency DQE[8] defined as:

$$DQE = \frac{(signal/noise)^2_{out}}{(signal/noise)^2_{in}} \quad . \qquad (1)$$

The relative uncertainty in the output signal S_o can be shown to be:

$$\frac{\sigma_o}{S_o} = [(DQE)\ S_i]^{-1/2} \qquad (2)$$

where S_i is the input signal. Thus, DQE can be thought of as the efficiency with which the input photons are utilized by the detector to affect the statistical precision. When the conversion efficiency is near unity, one can expect a DQE>0.3 or the uncertainty in the output signal to be less than two times the statistical uncertainty in the input x rays, i.e., $<2S_i^{-1/2}$. While DQE is somewhat lower when E is near unity, this is more than offset by the increase in the pixel x-ray saturation capacity.

4. CCD Architecture

Certain CCD architectures provide for simultaneous readout[9] which is tantamount to increased readout rate. A full-frame CCD is shown schematically in Fig. 3 (top). Readout is accomplished by a serial process whereby one line (i.e., one pixel from each column) is shifted into the horizontal register and then one pixel at a time is shifted out to the video amplifier. If four such CCDs are made contiguous on one chip as shown on Fig. 3 (bottom), and are independently clocked so that the four quadrants can be read out simultaneously, the effective readout is four times faster. A frame-transfer CCD is shown schematically in Fig. 4 (top). An image is acquired in the upper

half. At the end of the exposure, the image is rapidly transferred to the lower half which is the masked storage area. While the next image is acquired in the upper half, the previous image in the storage area is read out in the conventional manner as shown in Fig. 3 (top). If the exposure time is longer than the readout time, the readout does not slow down the the framing rate or introduce any deadtime. Shorter exposure could be obtained if the CCD had parallel readout as shown in Fig. 4 (bottom). Here each column has a video amplifier so that all the columns are read out simultaneously thereby eliminating the need for a serial register and therefore reducing the readout time by a factor equal to the number of columns. For practical considerations a parallel readout CCD cannot be made as large as a serial device as it would require an unreasonable number of video channels, i.e., amplifiers, ADCs, etc. Experimental devices of 128x64 pixels with parallel readout have been made by Tektronix (TK064PF).

5. CCD Control

The operation and much of the performance of a CCD is governed by the CCD controller. Since the controller determines such parameters as readout rate, exposure time, and frame size, its design is critical in the applications of CCDs. The basic scheme of our CCD controller is shown in Fig. 5. It was designed specifically for applications in synchrotron radiation research and similar scientific applications.

Data acquisition in a CCD and subsequent readout require a sequence of many operations which can be grouped into three major categories. The exposure and frame control determine such

parameters as exposure time, number of frames in a sequence, and frame size. The parallel register controller generates the sequence of gate signals which shift the charge in all columns in parallel, line by line, into the serial (horizontal) register. The serial register controller generates the sequence of gate signals which shift the charge, pixel by pixel, through the video amplifier, signal processing circuits, and ultimately into the ADC. The selection of a given sequence and its synchronization with other sequences is performed by the main CCD program controller. Thus for example, the program for reading out an image requires a parallel shift of one line followed by multiple serial shifts and analog to digital conversions which are then followed by the next parallel shift, etc. Each of the above three programmable controller units which make up the core of the CCD controller is essentially a command sequence generator. It is comprised of a RAM (random access memory) and output latch operating at a specified clock frequency, where some of the output signals are fed back to the input address of the RAM. The output command, or next state, is therefore determined by the current state as well as by the inputs to the RAM.

The clock frequency of the main CCD program controller is 20 MHz. Since the readout of a pixel requires a sequence of commands, the maximum readout rate is 5×10^6 pixels/s or ~50 ms for reading out a 512^2 pixel CCD. The parallel registers can be shifted at a maximum rate of 1 line/μs. Thus, for 10 pixel wide frames, the framing rate would be 10^5 frames/s. In addition to specifying the frame size, one can also select the effective size

of a pixel by specifying the binning factor. When binning by two the charge from two pixels is summed into a single well. When binning by two in the parallel register and in the serial register the effective pixel size is 2x2 real pixels, with a corresponding increase in well capacity and decrease in readout and digitization noise. Since this improvement in well capacity and dynamic range is obtained at the expense of spatial resolution, one would use a CCD with more pixels than required in this mode.

All the parameters such as frame size, readout rate, framing rate, and exposure time can be specified via the computer. Similarly, the program of operations can be specified via the computer, e.g., readout following each frame exposure or exposure of a sequence of frames, without interruption, with readout of the entire sequence following the exposure of the last frame. Thus it is seen that the CCD performance is critically dependent on the design and capabilities of the controller.

6. Applications of CCD-Based Detectors

Basic feasibility experiments were conducted with a prototype detector incorporating a 320x512 pixel CCD (RCA SID501EX). Results from experiments in protein crystallography and electron energy-loss spectroscopy (EELS) are reported. Since extended electron-loss fine structure (EXELFS) is the electron analog of extended x-ray absorption fine structure (EXAFS), array detector considerations are similar and therefore the results from the EELS experiments are pertinent to this paper. The following discussion will concentrate primarily on the CCD performance in the key areas considered in the preceding

sections, i.e., readout and framing rate, time-resolved measurements, DQE, and dynamic range.

6.1 Protein Crystallography

Protein crystals are extremely labile when exposed to x rays, seldom lasting more than two days in the beam of conventional x-ray sources. Since protein crystals diffract weakly, one to two weeks of data collection may be required to record a complete 3-dimensional data set, so that data from many crystals must be merged. It should be possible to collect data much faster with synchrotron radiation so that an entire 3-dimensional data set could be obtained from just a single crystal, if a suitable detector were available.

The useful life of a typical protein crystal in an intense synchrotron x-ray beam is 2-3 min. We propose to record a complete data set on about 90 image frames each of 1^{o} crystal rotation, within 3 min, which should yield a complete data set in all but the most demanding studies. This calls for data accumulation, readout, and storage of 90 frames in 2-3 min, which requires a data acquisition time of 1-2 s/frame.

We report here the development of a CCD-based area x-ray detector for protein crystallography, with which we have now conducted basic feasibility experiments. We have evaluated this detector by recording diffraction patterns from hen egg-white lysozyme protein crystals, using x rays from a conventional rotating anode generator[10]. From the results of this experiment we project the design parameters for a detector to be used in protein crystallography with x rays from advanced synchrotron

sources such as the 7-GeV synchrotron being designed at Argonne. The CCD-based detector system, as used in the protein crystallography experiment with a rotating anode x-ray generator, is shown schematically in Fig. 6. X rays scattered from the protein crystal form a diffraction pattern on the Gd_2O_2S:Tb (P-43) input phosphor which is then intensified with a two-stage, generation I image intensifier (Varo 1268) having unity magnification. A 2-lens system demagnifies the intensified image by 4 and focuses it on the CCD which is cooled to -35°C. At the end of the exposure time the controller initiates a CCD readout and the video signals are digitized and stored on the computer disk. The image intensifier used here may not be required when the detector is used with synchrotron radiation. Since the x-ray intensity from the rotating anode generator is considerably lower than that from a synchrotron, much longer exposure times are required which, in turn, could result in substantially higher CCD dark-current noise. The image intensifier is used here to assure adequate signal-to-noise ratio for weak signals.

A photograph of the experimental setup described in Fig. 6 is shown in Fig. 7. The detector system is mounted at the Elliot GX20 rotating anode generator and a CuK_α emission line is used. The generator was operating with a 200 μm focus, 40 kV, and 40 mA beam current. The x-ray beam was monochromated with graphite. The phosphor was 45 mm from the crystal. The crystal was mounted on the ø spindle of an Enraf Nonius rotation camera. With the detector lens removed, the CCD can be seen through the cryostat glass window (Fig 8).

A diffraction pattern was obtained with the CCD test

detector shown in Figs. 6 and 7. The crystal sample of tetragonal hen egg-white lysozyme was 0.5x0.5x0.1 mm^3. It was rotated through an angle of 2^o during the course of the exposure. The x-ray beam was defined by an adjustable collimator to match the crystal size (~0.5x0.5 mm^2). The diffraction pattern obtained in 14 min is shown in Fig. 9. For comparison a 60 min exposure on film (Kodak DEF-5) is shown in Fig. 10. Both the detector and film were 45 mm from the crystal. Since the detector was only 40 mm in diameter, it could not capture the outer part of the diffraction pattern. The CCD image is seen to closely resemble the film image. However, the CCD image is of better quality than the film, as it has lower noise and higher dynamic range. The lens system showed considerable vignetting which is exhibited as off-center attenuation. In addition, CCDs have some pixel-to-pixel variation in sensitivity. To correct for these nonuniformities, an image of a uniform x-ray flood was obtained and normalizing factors relative to the average pixel contents were calculated for each pixel. Figure 9 is a normalized image obtained by multiplying the pixel signals in the raw image by these factors.

The virtues of a real-time video display are readily apparent. Although film displays continuous variation in intensity, relative peak intensities are not easily perceived. A video display (Fig. 9) can instantly project X and Y cuts which show peak profiles with which spots can be evaluated at a glance with respect to intensity and shape.

The operation of the test detector with our rotating anode

x-ray generator was evaluated in terms of several performance criteria and the results are listed in Table 1. The x-ray flux on the detector, 10^4 ph/s, was obtained from the integral of the full image in Fig. 9, which includes the diffraction peaks and the diffuse background. The intensity of the incident beam, $2x10^7$ ph/s, was measured with a calibrated phosphor-photomultiplier detector. From these measurements the scattering efficiency of the lysozyme crystal in this experiment geometry was found to be about 10^{-3}, typical of protein crystals.

The maximum count in a peak, $6x10^4$ x rays, corresponds to the peak saturation-capacity. When one or more pixels in a peak reach the full well level the peak is said to have maximum x-ray count capacity or saturation capacity. The correspondence between x-ray counts in the peak and electrons in the CCD pixel well is determined by the conversion efficiency E which is the CCD electron yield per x-ray photon on the input phosphor. A value of E = 90 e^-/ph was obtained from the integral of a peak due to an x ray beam of known intensity incident on the input phosphor for a controlled exposure time. The maximum exposure time, or accumulation time per frame, 860 s, was determined from the peak saturation-capacity and the x-ray intensity of the strongest peak, 60 ph/s. If the peak is situated on a background, the exposure time must be reduced accordingly to avoid pixel overflow.

The dark current background of the CCD at -35°C and with 860 s exposure, was approximately 4% of the saturation level, corresponding to ~120 e^- rms dark current noise per pixel. The CCD read noise and the digitization noise were 60 e^-/pixel and 42

e^-/pixel, respectively. The total electronic noise due to the CCD dark current, CCD readout and the ADC digitization (image intensifier excluded) was calculated to be $2x10^{-4}$ of a saturation peak. The uncertainty due to these fluctuations is considerably less than that due to the x-ray Poisson statistics in the peak $(6x10^4)^{-1/2}$. Such a small contribution of detector noise to the uncertainty of the output signal is expected when the conversion efficiency E>>1, as for this case DQE ≈1.

The dynamic range, defined as the ratio of the integral of the strongest peak to the rms fluctuations in the background over the same area (81 pixels) was $2x10^2$, lower than expected due to the unusually high background of the image intensifier in the test detector system.

The evaluation of the test detector provides the necessary data to project the performance of a detector for protein crystallography with synchrotron x rays. The increase in flux from the synchrotron source as compared with that from a rotating anode generator is the paramount factor to be considered. The expected flux on a 0.5x0.5 mm^2 crystal from a bending magnet of the 7-GeV synchrotron being designed at Argonne[11] is $2x10^{12}$ x-ray photons/s (Table 1). This corresponds to 10^5 increase in x-ray intensity and would subject the detector to a flux of $4x10^9$ x-ray photons/s, comparable to the intensity observed in the EELS experiments (Table 2).

From Figs. 9 and 10 it is apparent that a detector with a lateral dimension of 80 mm will be more adequate than one with only 40 mm. Using a 512x512 pixel CCD (14x14 mm^2) with an 80 mm

detector would give nearly the same spatial resolution as that obtained with the 40 mm test detector and 314x316 pixels (9.5x9.5 mm^2). A demagnification of ~6 would be required for the 80 mm detector as compared to 4 which was used in the test detector.

The ultimate limit of precision in this protein crystallography detector is determined by the uncertainty due to the x-ray Poisson statistics and, in turn, by the peak saturation capacity. In order to obtain the maximum x-ray count in a given (short) exposure time, the conversion efficiency should be near unity (Sec. 3). Scaling the value obtained with our test detector (Table 1) by the lower conversion efficiency we obtain a peak saturation capacity of over $3x10^6$ x-ray photons and DQE = 0.4. From Eq. 2 we obtain a statistical uncertainty of ~0.1% for a saturation peak.

For a lysozyme crystal the strongest peak would have an intensity of $6x10^6$ Xph/s and would reach saturation in 550 ms. With this accumulation time of ~0.5 s/frame and conventional data storage time of ~1 s for a $0.5x10^6$ byte frame, the CCD readout rate need not be faster than 0.5 s/frame in order to meet our data acquisition objective of 1 frame/s. At this readout rate (0.5 Mpixel/s) the read noise is ~100 e^- rms/pixel and the total electronic noise is $2x10^{-4}$ of the saturation peak which is only 1/5 of the statistical uncertainty discussed above.

Thus, based on the detector performance with rotating anode x-ray generator, we project that with an x-ray intensity $>10^9$ photons/s on the detector, as expected from a synchrotron source, one can obtain a complete 3-dimensional set of reflections in 2-3 min, with a statistical precision <1%. This should virtually meet

all detector requirements for protein crystallography.

6.2 EXELFS/(EXAFS)

In recent years there has been an increasing interest in improving the data collection efficiency in EELS and EXAFS. At the present time EELS data is recorded by scanning the electron spectrum across a slit viewed by a scintillator-photomultiplier detector and storing the data in a computer. Instead of scanning the electron beam across an exit slit and measuring the EELS spectrum point by point with a single detector, one can use an array detector in a parallel detection mode (without a slit) and improve the efficiency by more than 100 fold[12-14]. A similar technique has been introduced in EXAFS. Instead of rotating the monochrometer and changing the energy of the incident x-ray beam step by step, one can use a bent crystal to focus the x rays on the sample and measure the dispersive EXAFS spectrum with an array detector[15,16].

The parallel detection system currently being develcped for EELS is shown schematically in Fig. 11. An electron spectrometer (Gatan 607) is mounted at the end of the electron optical column of a transmission electron microscope (Philips EM420). At the spectrometer image plane, one observes an intense peak E_o corresponding to those electrons which have suffered no or negligible energy loss in passing through the specimen of interest. Displaced from this peak by a distance x one observes a spectrum of electrons which have lost varying amounts of energy due to interaction with the sample. The distance is $x = \mu\Delta E$, where μ is the spectrometer dispersion and ΔE is the energy loss.

Typical values of μ range from 0.5 to 2 μm/eV, depending upon the microscope operating voltage. The spatial extent of a 1000 eV spectrum therefore ranges only from 500 to 2000 μm. Since the typical pixel size of a CCD is 20-30 μm, it is necessary to magnify the spectrum to match the desired spectral resolution to the number of pixels in the CCD. To accomplish this an electromagnetic quadrupole doublet lens was built allowing one to continuously vary the dispersion of the image on the YAG:Ce scintillator from 20-800 μm/eV. An optical lens system consisting of two camera-type lenses (Nikon, 50 mm, f/1.2) mounted nose to nose (magnification=1), projects the image from the scintillator onto the CCD, which was thermoelectrically cooled to -30^{o}C. A photograph of the experimental system is shown in Fig. 12. The data from the CCD was read out into a PDP 11/73 computer to give the energy loss spectra.

The data acquisition scheme for recording 1-dimensional electron energy-loss spectra on an area CCD is shown in Fig. 13. An opaque mask covers all the CCD pixels except for one 5x512 pixel frame (left side of CCD) which remains light sensitive. Electrons impinging on the YAG:Ce scintillator (Fig. 11) are focused by the optical lens on the sensitive area of the CCD (Fig. 13). Once the pixels corresponding to the most intense peak approach saturation, the charge in the exposed area is shifted in 5-10 μs to the masked region of the CCD and data acquisition continues in the exposed area. With 512 pixel rows, 102 complete frames can be recorded in the CCD in one continuous exposure without data loss due to readout. Readout begins once the last frame is recorded. Binning each group of 5 parallel-register

pixels reduces the readout time by 5 and also increases the signal-to-readout noise ratio. Corresponding pixels in successive frames may be summed in the computer memory to increase the dynamic range for data acquisition beyond that of a single CCD frame.

In the experiments reported here we deviated slightly from the scheme shown in Fig 13. Instead of offsetting the CCD with respect to the scintillator, they remained aligned as shown in Fig. 11. The image, however, was displaced left of the scintillator center using the deflection coil shown in Fig. 12 (left of the electron lens). A series of frames showing electron energy-loss spectra in boron nitride taken in one continuous exposure (without readout in between frames) is shown in Fig. 14. An X cut (below) through one frame shows the spectrum with the boron K edge (energy loss increases from right to left). Individual pixels are clearly resolved which shows that the YAG:Ce scintillator did not limit the CCD spatial resolution.

A set of five frames, taken from a sequence made in a continuous exposure, showing the zero-loss peak (E_o) is shown in Fig. 15. An X cut of the center peak is shown below and a Y cut, corresponding to the Y cursor position, is shown on the left. The E_o peak position fluctuated during the measurement from right (at bottom) to left (at center) and to right again (at top). This shows more clearly in the Y cut were the the center peak (closest to the Y cursor) has the highest amplitude. These fluctuations are even more apparent in Fig 16 which shows more frames of the above E_o spectra sequence. These fluctuations were caused by

interference of the AC magnetic field in the room with the electron microscope/spectrometer optics. The Y cut shows that the fluctuations have a period of ~8 ms which corresponds to the 60 Hz power-line frequency. The exposure time for each frame was ~0.8 ms. Although this experiment was not planned, the lessons learned were valuable. In the present context it demonstrates the effectiveness of the CCD in recording time-resolved phenomena.

In EELS as well as in EXAFS the small fine structure oscillations in the spectrum are of principal interest. Since these are usually <10% of the continuum on which they are superposed, minimizing statistical fluctuations are of crucial importance. We sought to determine the effect of detector noise on the overall measurement uncertainty. One pixel, with charge corresponding to 20% of full well, was noted in 40 separate frames similar to those shown in Fig. 14. The fluctuations in the pixel readouts had a relative standard deviation of 0.4%. These frame-to-frame fluctuations reflect the uncertainty due to Poisson statistics in the beam current (shot noise), the uncertainty due to detector noise, and drift in the electron microscope during the ~1 min measurement of 40 frames where each frame was exposed for 1.68 s. To assess the <u>detector</u> contribution to the uncertainty, we calculated the relative uncertainty in the measured pixel value from the detection statistics and electronic noise. The detector contribution is effected by the conversion efficiency E. When E>>1, the detector contribution is negligible and the uncertainty σ_o in the detector output signal S_o is virtually entirely due to Poisson

statistics in the input beam current S_i, i.e., $\sigma_o/S_o \approx S_i^{-1/2}$. However, for effective use of CCDs with intense flux of electrons or x rays, E should not be much larger than unity (Sec. 3) and σ_o/S_o is therefore somewhat higher than this as indicated by Eq. 2.

The conversion efficiency E was determined from a zero-loss spectrum similar to those shown in Fig. 15. The integral of the spectrum gives the number of CCD electrons e_o and the input current, 0.5 nA, integrated over the exposure time gives the number of input electrons e_i. The conversion efficiency E is $e_o/e_i = 2.6$. This in turn gave a scintillation efficiency for the YAG:Ce of 500 photons/e^-@100keV. Using this value of E in combination with the measured rms dark current noise of 40 e^-, rms read noise of 50 e^-, and rms digitization noise of 45 e^- we calculated $\sigma_o/S_o = 1.5\ \sigma_i/S_i$ for S_o = 20% of pixel saturation value[7]. Thus, this experiment shows that a system with conversion efficiency near unity is a viable design where the detector contribution to the measurement uncertainty is comparable to or less than that due to the Poisson statistics in the incident beam. The beam current of 0.5 nA corresponds to 3×10^9 e^-/s which is nearly the same intensity as the photon flux expected on the detector in protein crystallography with the 7 GeV synchrotron (Table 1).

The figure of merit for the efficiency of an array detector as pertaining to statistical precision is given by DQE. Using the above results $\sigma_o/S_o = 1.5\ \sigma_i/S_i$ and Eq. 2, we obtain DQE=0.4. Thus, with this array detector one would have to count 2.5 times

longer than a single detector (DQE=1) would count at any one point in order to obtain the same statistical precision per pixel (Eq. 2). A 500 pixel detector would therefore be 200 times (500/2.5) more efficient in collecting a 500 point EELS/EXAFS spectrum than a single detector counting one point at time.

The dynamic range was also determined from a zero-loss spectrum. The ratio of the integral of the peak (4x5 pixels) to the square root of the background noise in 20 pixels, gave a dynamic range of $7x10^3$. When a series of m frames are summed in the computer memory, the dynamic range would increase in proportion to $m^{1/2}$. Thus, for a combined spectrum of 100 frames (Fig. 13) the dynamic range can be expected to be $7x10^4$. The results from the EELS experiments discussed above are summarized in Table 2.

7. Conclusion

A CCD is a suitable and an effective sensor for synchrotron x-ray detectors. It was evaluated experimentally in two different areas. In protein crystallography, diffraction patterns of a lysozyme crystal were obtained with a rotating anode x-ray generator. When the results obtained are extrapolated to the case of a synchrotron source, images can be expected at a rate of 1 frame/s with a statistical uncertainty in a diffraction spot of 0.1%. In EELS, energy-loss spectra have been recorded in a parallel detection mode with an efficiency of 200x that of a single channel detector. This efficiency is based on a DQE=0.4 obtained from a measured sequence of 40 spectra. The use of the detector in recording time-resolved phenomena is demonstrated in a series of frames showing the power line

generated stray magnetic field modulating the electron microscope/spectrometer optics. Results similar to those obtained in the EELS experiments can also be expected in dispersive EXAFS, as EXELFS is the electron analog of EXAFS.

Cost effectiveness has been an important consideration in the conceptual design of this detector system. It is based on the use of commercially available components in a programmable system which can reconfigured to meet different scientific applications without having to redesign the system. Future research is expected to concentrate on detector configurations which will best meet specific applications.

Acknowledgments

The authors gratefully acknowledge the contribution of A. E. Scandora, who wrote the image display programs, and M. R. Strelau, who documented the design and operation of the CCD controller.

References

[1] "7-GeV Advanced Photon Source: Conceptual Design Report", Argonne National Laboratory report ANL-87-15 (April 1987).

[2] R. A. Dalglish, V. J. James and G. Tubbenhauer, Nucl. Instr. Methods 227 (1984) 521.

[3] E. F. Eikenberry, S. M. Gruner and J. L. Lowrance, IEEE Trans. Nucl. Sci. NS-3(1) (1986) 542.

[4] Charge-Coupled Devices and Systems, Eds. M. J. Howes and D. V. Morgan (John Wiley & Sons, New York, NY, 1979).

[5] Charge-Coupled Devices and Their Applications, Eds. J. D. E. Beynon and D. R. Lamb (McGraw Hill, London, UK, 1980).

[6] H. W. Deckman and S. M. Gruner, Nucl. Instr. Methods A246 (1986) 527.

[7] M. G. Strauss, I. Naday, I. S. Sherman and N. J. Zaluzec, Ultramicroscopy 22 (1987) 117.

[8] S. M. Gruner, J. R. Milch and G. T. Reynolds, IEEE Trans. Nucl. Sci. NS-25(1) (1978) 562.

[9] R. D. McGrath, D. E. Russel, J. Frank and S. Popik, in: Proc. Electron Imaging 85 Conf. - 1985, (Institute for Graphic Communication, Boston, MA, 1985) p. 156.

[10] M. G. Strauss, I. Naday, I. S. Sherman, M. R. Kraimer and E. M. Westbrook, IEEE Trans. Nucl. Sci. NS-34(1) (1987) 389.

[11] "6-GeV X-Ray Source: Conceptual Design Report", Supplement B, Argonne National Laboratory report LS-51, (March 1986) p. 71.

[12] D. E. Johnson, K. L. Monson, S. Csillag and E. A. Stern, in: Analytical Electron Microscopy - 1981, Ed. R. H. Geiss (San Francisco Press, San Francisco, CA, 1981) p. 205.

[13] R. F. Egerton, J. Electron Microsc. Tech. 1 (1984) 37.

[14] C. L. Krivanek, C. C. Ahn and R. B. Keeny, Ultramicroscopy 22 (1987) 103.

[15] R. P. Phizackerley, Z. V. Rek, G. B. Stephenson, S. D. Conradson, K. O. Hodgson, T. Matsushita and M. Oyanagi, J. Appl. Cryst. 16 (1983) 220.

[16] A. M. Flank, A. Fontaine, A. Jucha, M. Lemonnier, D. Raoux and C. Williams, Nucl. Instr. Methods 208 (1983) 651.

Table 1

Results from Protein Crystallography Experiment

	Test Detector (Experiment values)	Synchrotron Detector (Projected values)
X-ray source	Rotating anode gen. (40 kV, 40 mA)	7-GeV synchrotron (bending magnet)
Photon energy (keV)	8	8
Beam intensity on crystal (Xph/s)	$2x10^7$	$2x10^{12}$
Lysozyme crystal size (mm^2)	0.5x0.5	0.5x0.5
Detector area (mm^2)	40x40	80x80
Frame size (pixels)	314x316	512x512
Detector flux (Xph/s/det. area)	10^4	$4x10^9$
Intensity of strongest diffraction peak (Xph/s)	60	$6x10^6$
Conversion efficiency (e^-/Xph)	90	1
Gd_2O_2S:Tb phosphor efficiency ph/Xph @ 8 keV	40	40
Detective quantum efficiency, DQE, for saturation peak	~1	0.4
Diffraction peak saturation capacity (Xph)	$6x10^4$	$3x10^6$
Dynamic range: saturation peak/rms noise	$2x10^2$	$5x10^3$
Accumulation time (s/frame)	860	0.55
CCD readout time (s/frame)	1	0.5
Framing rate (s/frame)	5	1

Table 2

Results from EELS experiments

Beam Current (nA)	0.5
(e^-/s)	$3x10^9$
Conversion Efficiency: No. CCD e^-/No. incident e^-	2.6
YAG:Ce scintillation efficiency (photons/e^-@100keV)	500
Statistical uncertainty of output signal vs. input signal	1.5
Detective quantum efficiency, DQE, for 20% saturation signal	0.4
Frame-to-frame pixel signal fluctuations (σ^-%)	0.4
Dynamic range: saturation peak/rms noise	$7x10^3$

Figure Captions

Fig. 1 Conceptual drawing of a frame-transfer CCD, where area A is for image acquisition and area B (covered with an opaque mask) is for image storage. Connections of the pixel electrodes are shown enlarged on left.

Fig. 2 Chart showing signal flow through components of CCD-based synchrotron x-ray detector.

Fig. 3 Schematic diagram of a full-frame CCD with serial readout (top) as indicated by arrows. When four such CCDs are on one chip (bottom) and are independently clocked, the four quadrants can be read out simultaneously.

Fig. 4 Schematic diagram of a frame-transfer CCDs. Upper CCD is read out serially pixel by pixel. Lower CCD, with a separate video amplifier for each column, is read out in parallel line by line.

Fig. 5 Drawing of basic CCD controller showing its three principal control functions the sequence of which is determined by the CCD program controller which operates at a clock frequency of 20 MHz that results in a readout rate of 5×10^6 pixels/s.

Fig. 6 Schematic diagram of CCD-based detector system as was used with rotating anode x-ray generator in a protein crystallography experiment.

Fig. 7 Photograph of CCD test detector system mounted on an Elliot GX20 rotating anode x-ray generator during a protein crystallography experiment as shown in Fig. 6.

Fig. 8 Photograph of CCD seen through the cryostat glass window when the lens (Fig. 7) was removed.

Fig. 9 Diffraction pattern, obtained with CCD test detector in 14 min, of a tetragonal hen egg-white lysozyme crystal rotating through 2^{o} during the exposure. X and Y cuts at cursor positions show the horizontal and vertical peak profiles which permit evaluation of the diffraction spots at a glance.

Fig. 10 Diffraction pattern, obtained on film in 60 min, of the same lysozyme crystal used with the CCD test detector in Fig. 7. This image is virtually identical to that in Fig. 9 except that the CCD detector was smaller than the film and therefore it could not capture the outer part of the diffraction pattern.

Fig. 11 Schematic diagram of CCD-based detector system as used with an electron microscope/spectrometer in a parallel detection mode in electron energy-loss spectroscopy (EELS).

Fig. 12 Photograph of CCD-based parallel detection system attached to a Gatan 607 electron spectrometer during an EELS experiment as shown in Fig. 11.

Fig. 13 Diagram showing data acquisition scheme for recording 1-dimensional electron energy-loss spectra in multiple frames on an area CCD.

Fig. 14 Images showing frames containing electron energy-loss spectra in boron nitride taken as shown in Fig. 13 in one continuous exposure without readout in between frames. X cut (bottom) at cursor position shows the

spectrum with the boron K edge (energy loss increases from right to left).

Fig. 15 Five frames of images showing the zero-loss peak (E_o) with X and Y cuts corresponding to cursor positions. Note the E_o peak fluctuations with respect to the Y cursor from right (at bottom) to left (at center) and to right again (at top). The fluctuations were due to interference of stray AC magnetic fields with the electron microscope/spectrometer optics.

Fig. 16 Series of images of zero-loss peak (E_o) as in Fig. 15 showing the E_o peak fluctuations to be periodic with an ~8 ms cycle time corresponding to the 60 Hz power-line frequency. With an exposure time of ~0.8 ms/frame, this image sequence demonstrates the effectiveness of the CCD in recording time-resolved phenomena.

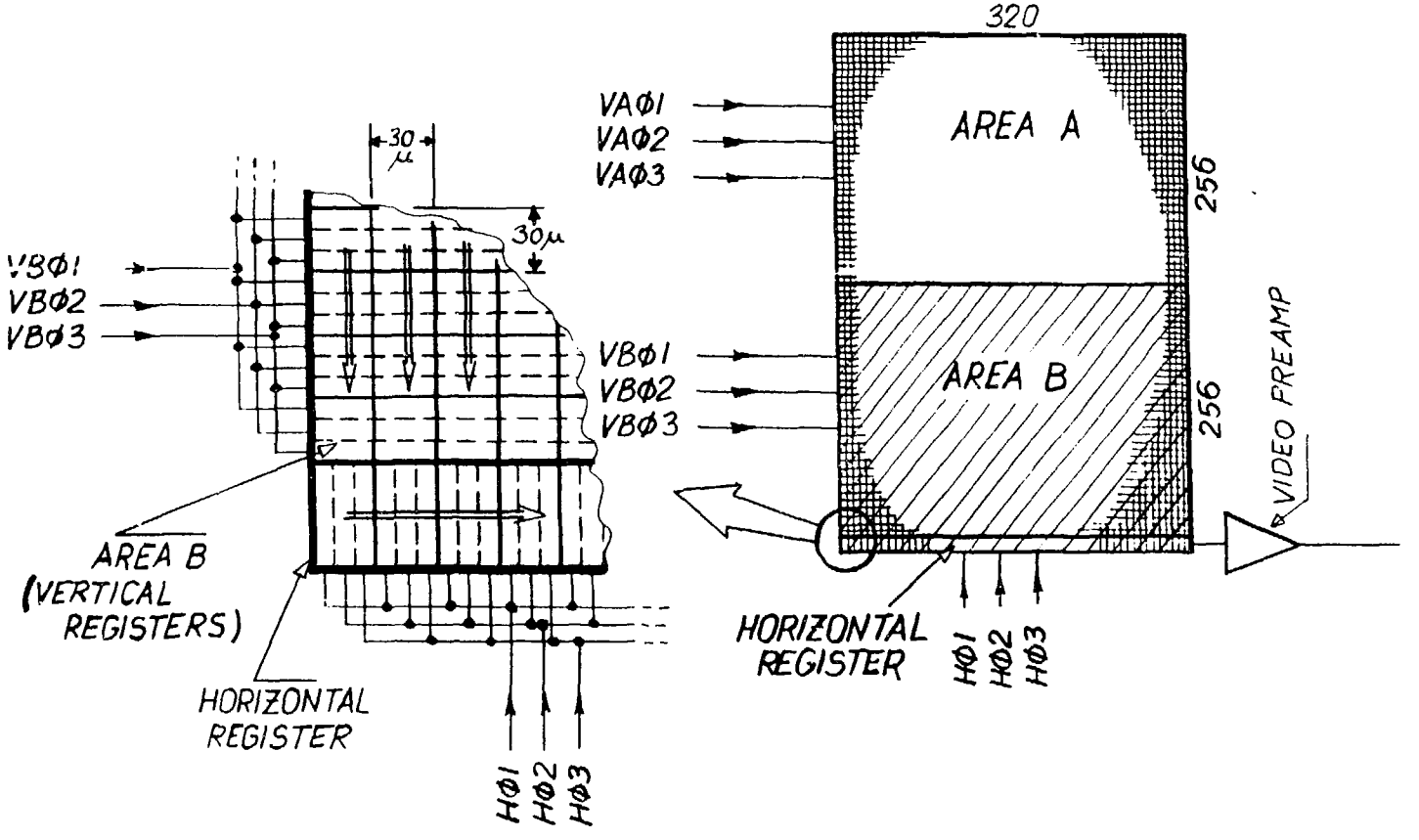
320
VAΦ1
VAΦ2
VAΦ3
AREA A
256
VBΦ1
VBΦ2
VBΦ3
AREA B
256
VIDEO PREAMP
HORIZONTAL REGISTER
HΦ1
HΦ2
HΦ3
30 μ
30μ
VBΦ1
VBΦ2
VBΦ3
AREA B (VERTICAL REGISTERS)
HORIZONTAL REGISTER
HΦ1
HΦ2
HΦ3

Fig. 1

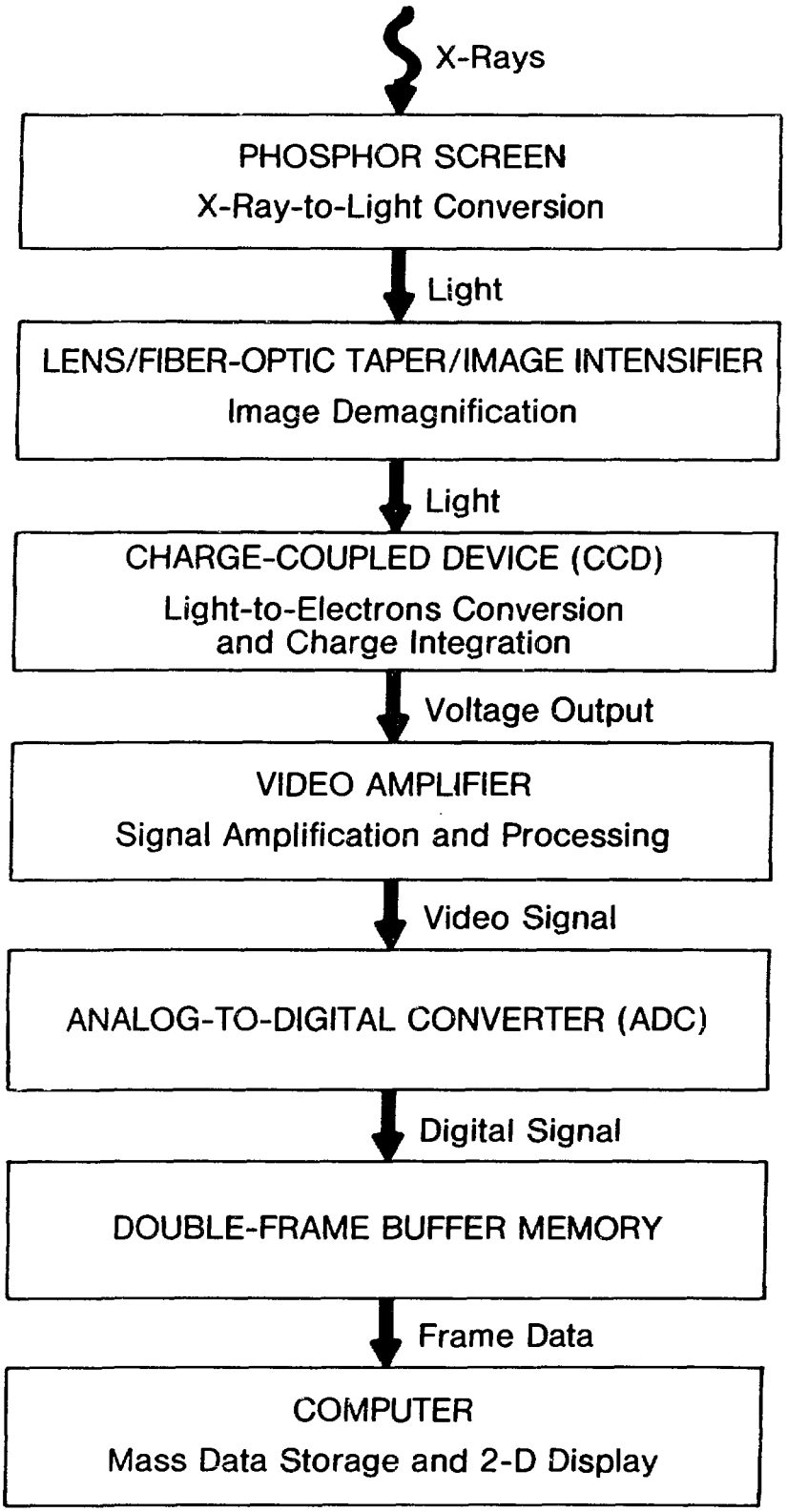
X-Rays
PHOSPHOR SCREEN
X-Ray-to-Light Conversion
Light
LENS/FIBER-OPTIC TAPER/IMAGE INTENSIFIER
Image Demagnification
Light
CHARGE-COUPLED DEVICE (CCD)
Light-to-Electrons Conversion
and Charge Integration
Voltage Output
VIDEO AMPLIFIER
Signal Amplification and Processing
Video Signal
ANALOG-TO-DIGITAL CONVERTER (ADC)
Digital Signal
DOUBLE-FRAME BUFFER MEMORY
Frame Data
COMPUTER
Mass Data Storage and 2-D Display

Fig. 2

Full Frame CCD

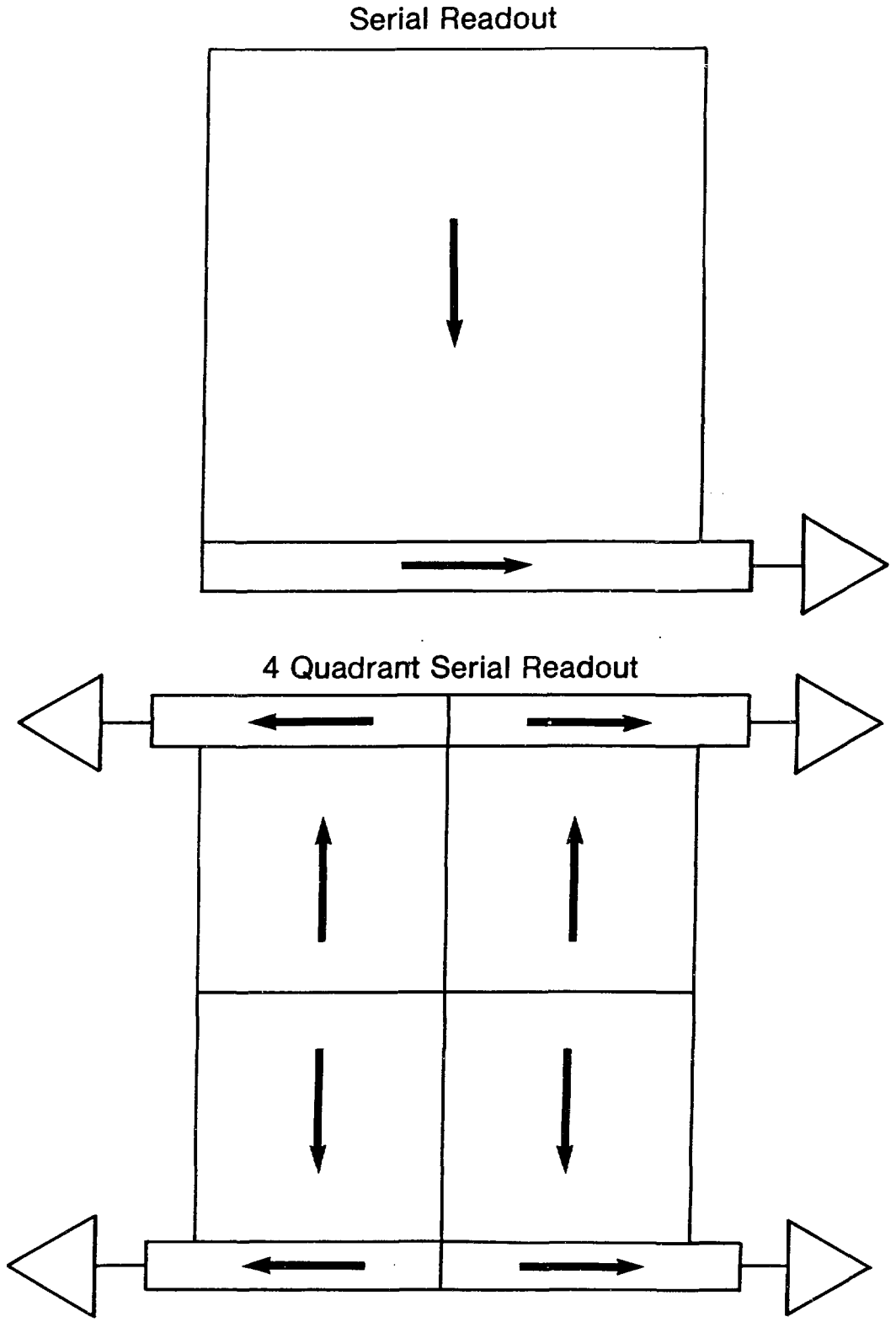

Fig. 3

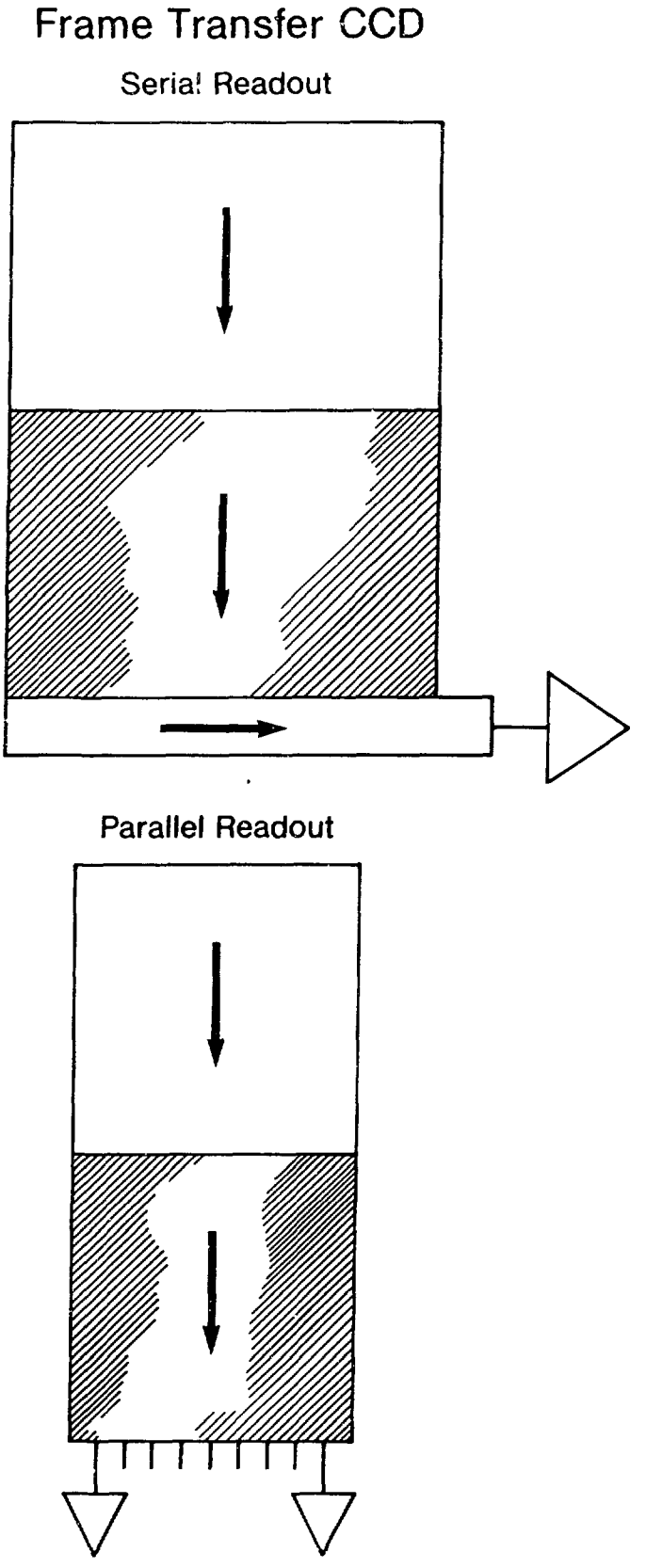

Fig. 4

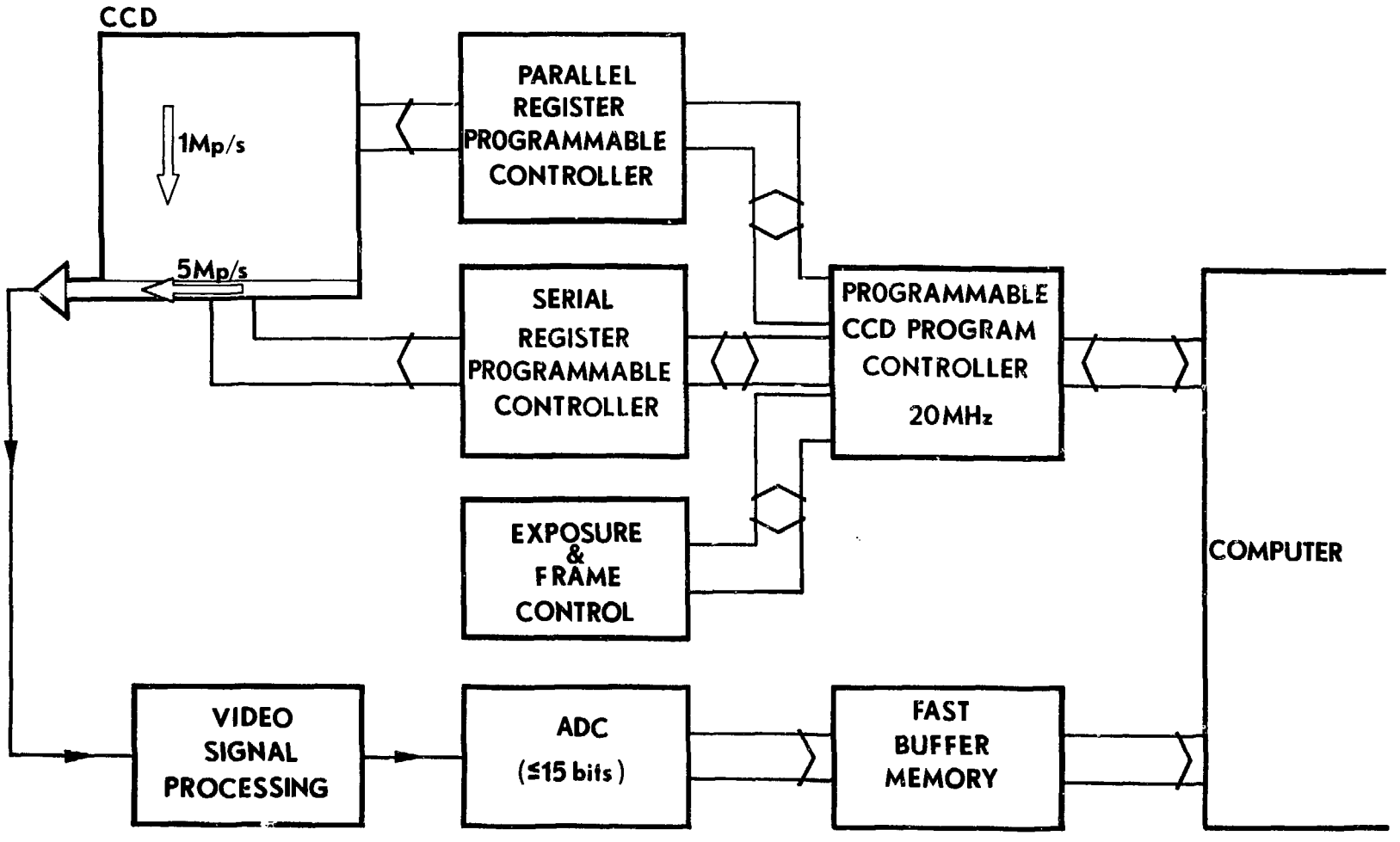
CCD
1Mp/s
5Mp/s
PARALLEL REGISTER PROGRAMMABLE CONTROLLER
SERIAL REGISTER PROGRAMMABLE CONTROLLER
EXPOSURE & FRAME CONTROL
PROGRAMMABLE CCD PROGRAM CONTROLLER 20MHz
COMPUTER
VIDEO SIGNAL PROCESSING
ADC (≤15 bits)
FAST BUFFER MEMORY

Fig. 5

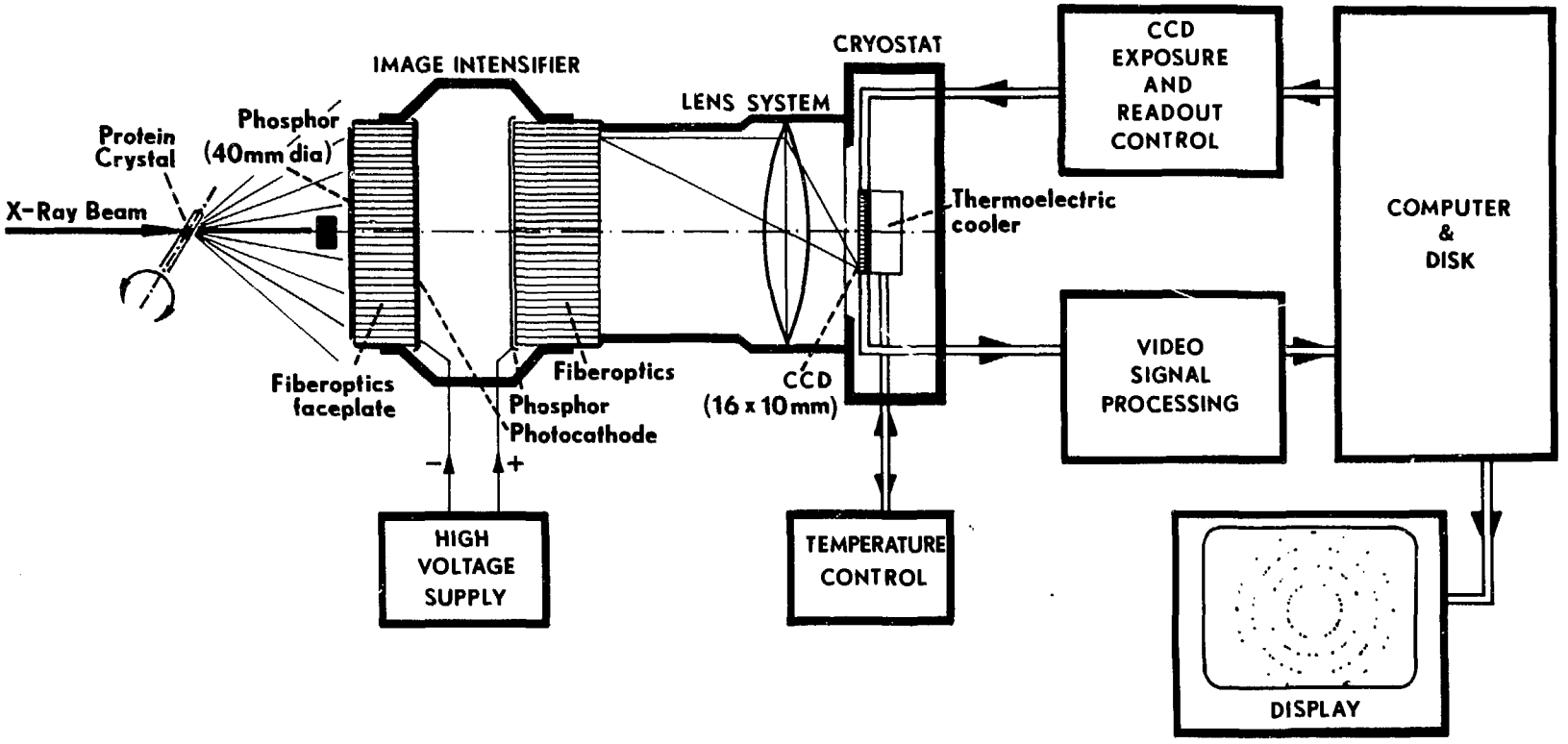
IMAGE INTENSIFIER
CRYOSTAT
CCD EXPOSURE AND READOUT CONTROL
COMPUTER & DISK
LENS SYSTEM
Protein Crystal
Phosphor (40mm dia)
X-Ray Beam
Thermoelectric cooler
VIDEO SIGNAL PROCESSING
Fiberoptics faceplate
Fiberoptics
Phosphor
Photocathode
CCD (16 x 10 mm)
HIGH VOLTAGE SUPPLY
TEMPERATURE CONTROL
DISPLAY

Fig. 6

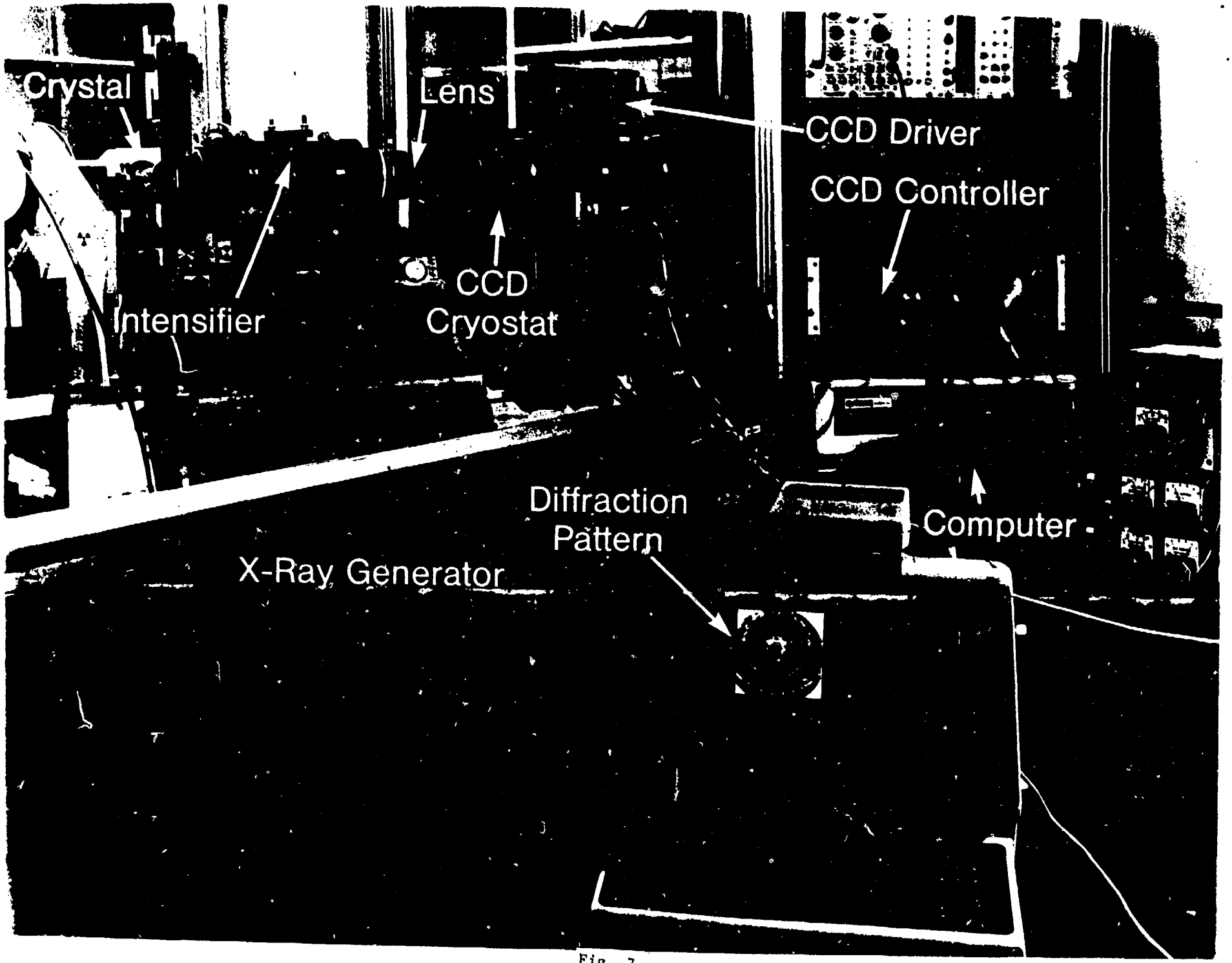
Crystal
Lens
CCD Driver
CCD Controller
Intensifier
CCD
Cryostat
Diffraction
Pattern
Computer
X-Ray Generator

Fig. 7

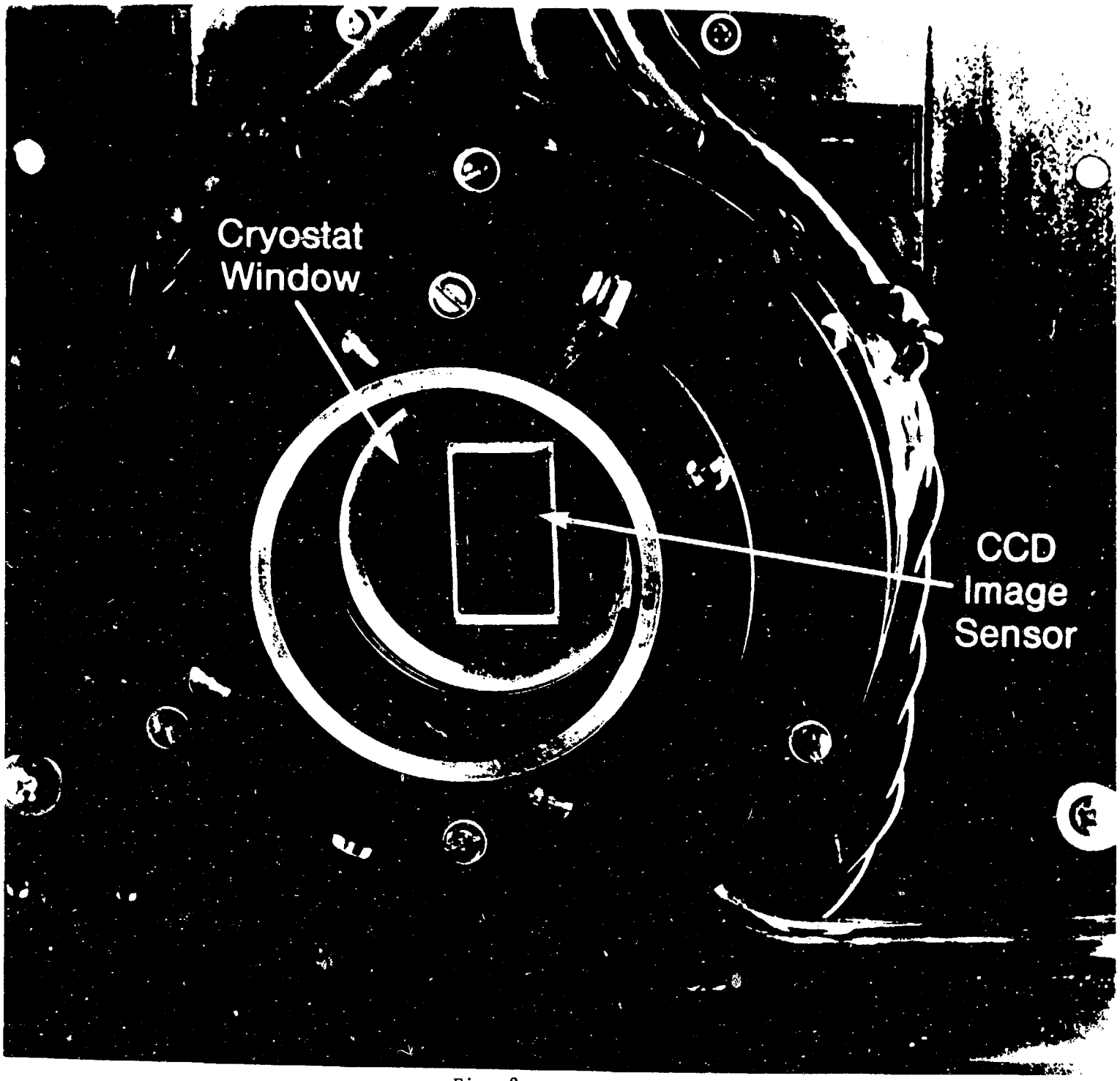

Fig. 8

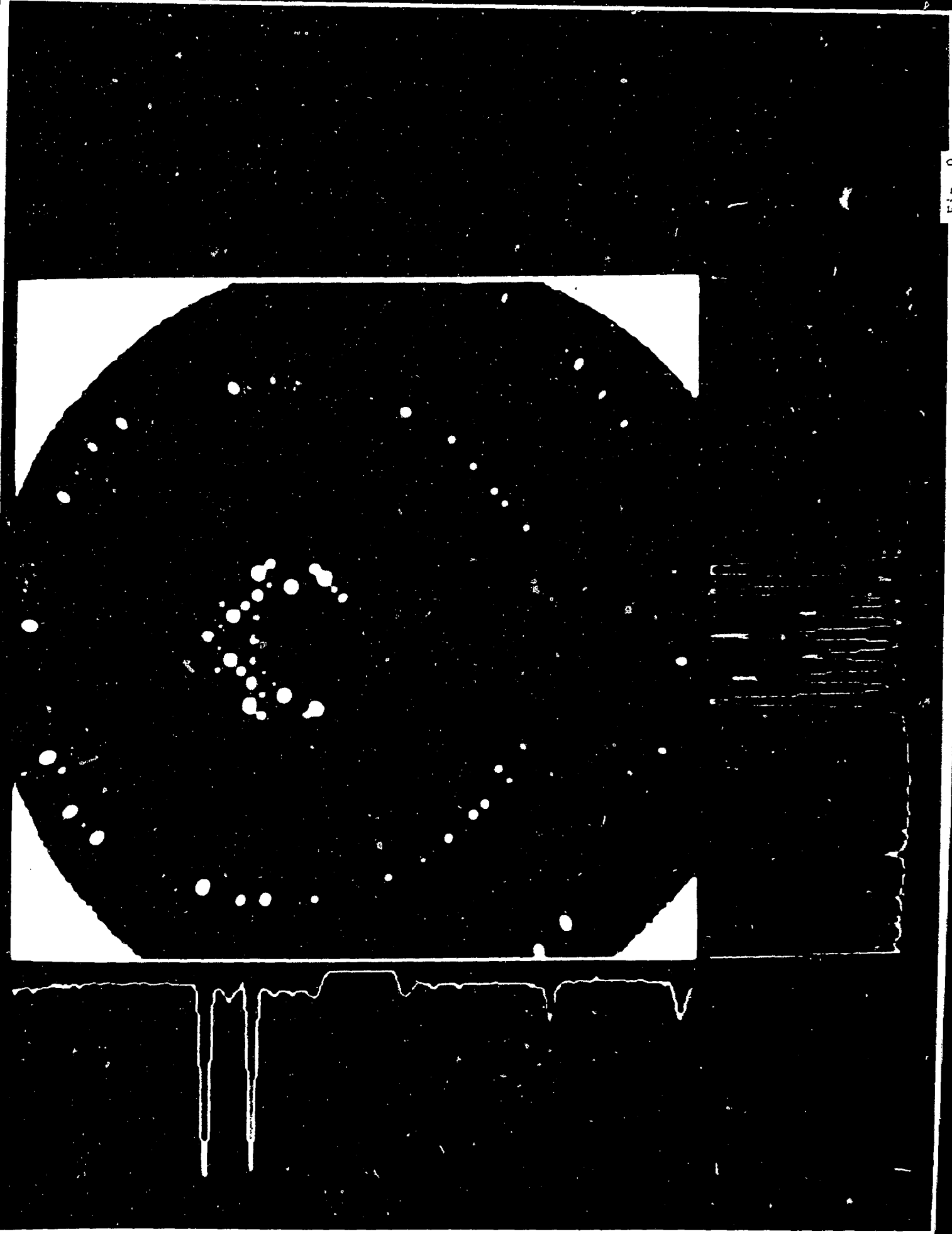

Fig. 9

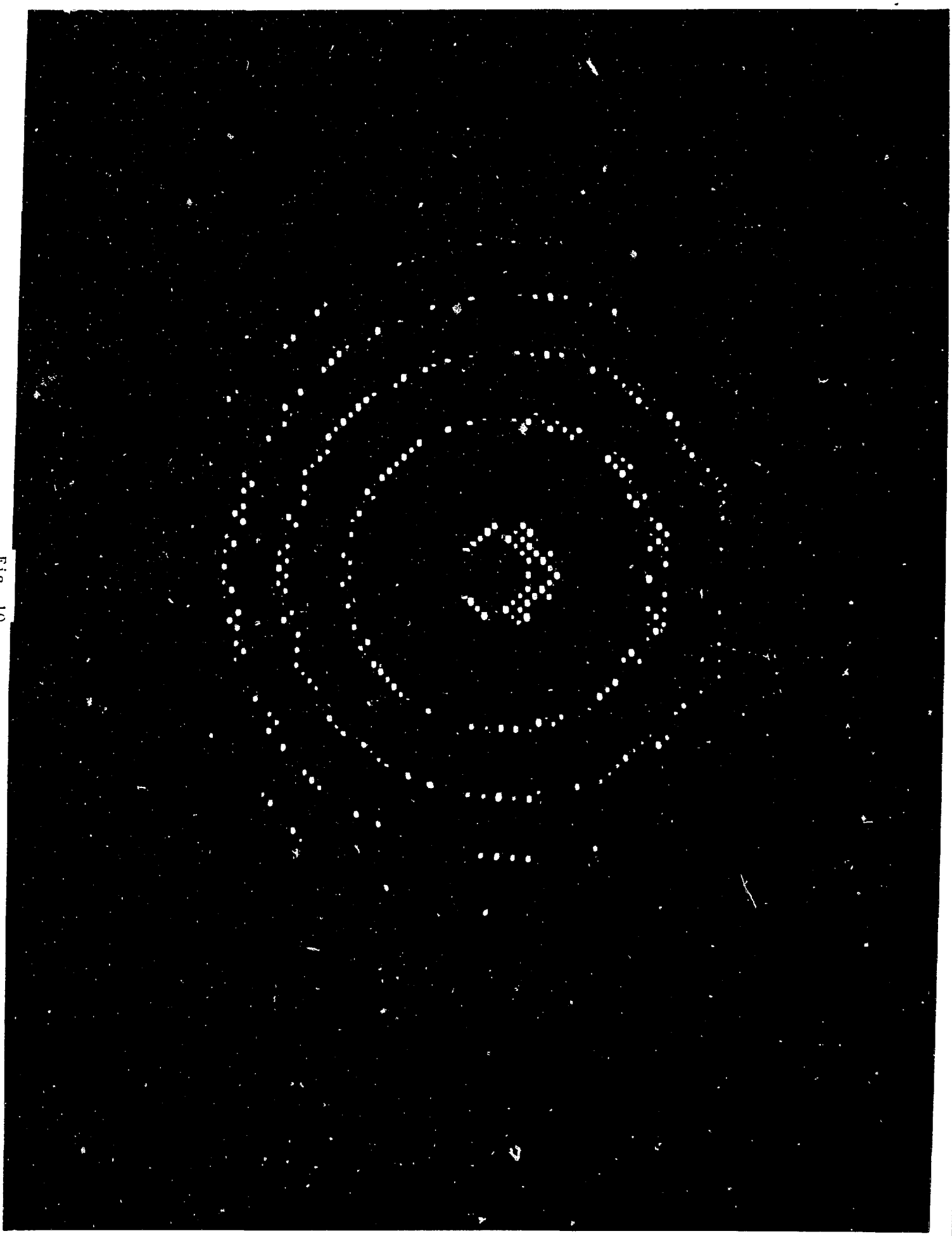

Fig. 10

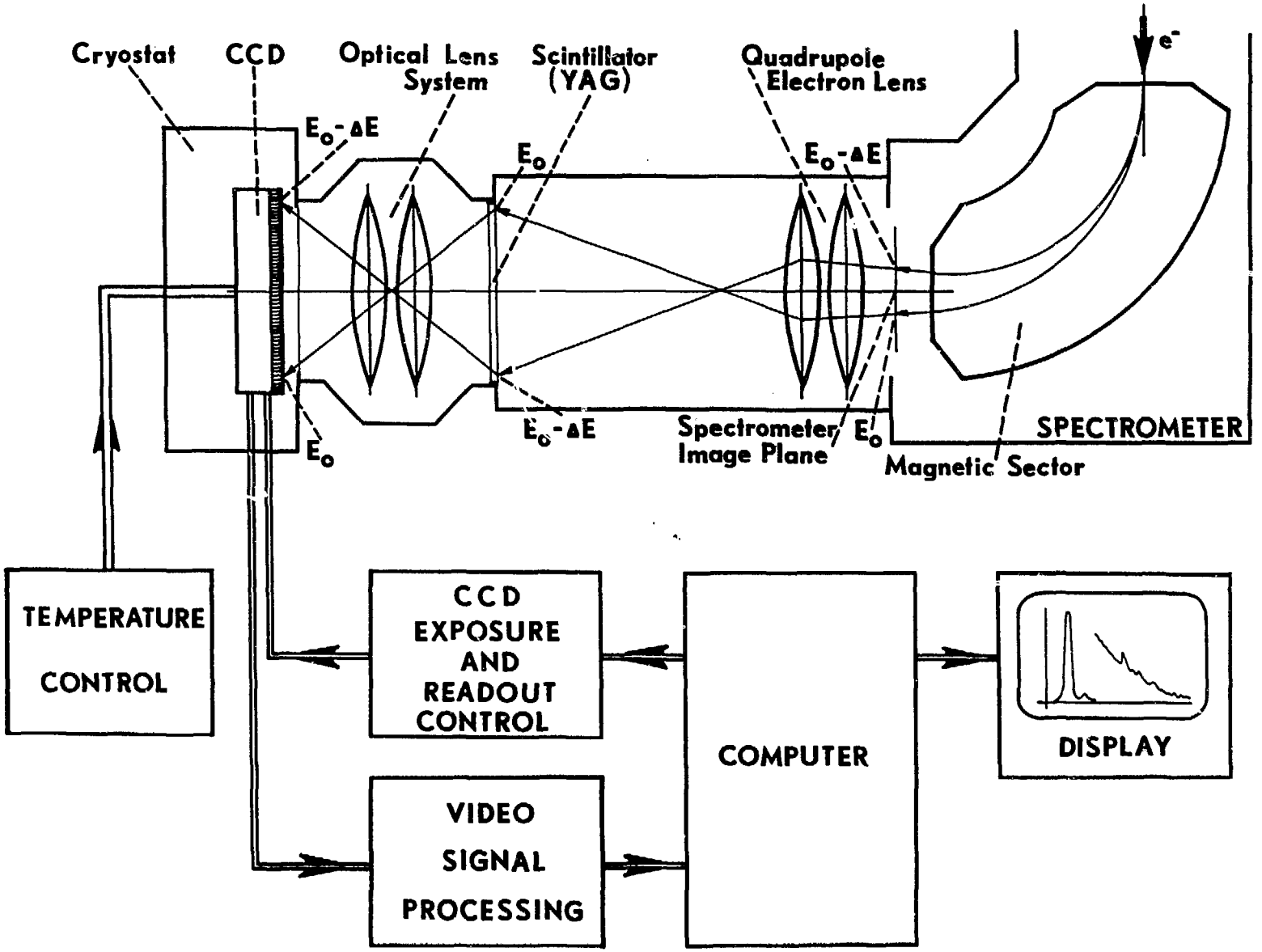
Cryostat
CCD
Optical Lens System
Scintillator (YAG)
Quadrupole Electron Lens
e⁻
$E_o - \Delta E$
E_o
$E_o - \Delta E$
E_o
$E_o - \Delta E$
E_o
Spectrometer Image Plane
Magnetic Sector
SPECTROMETER
TEMPERATURE CONTROL
CCD EXPOSURE AND READOUT CONTROL
COMPUTER
DISPLAY
VIDEO SIGNAL PROCESSING

Fig. 11

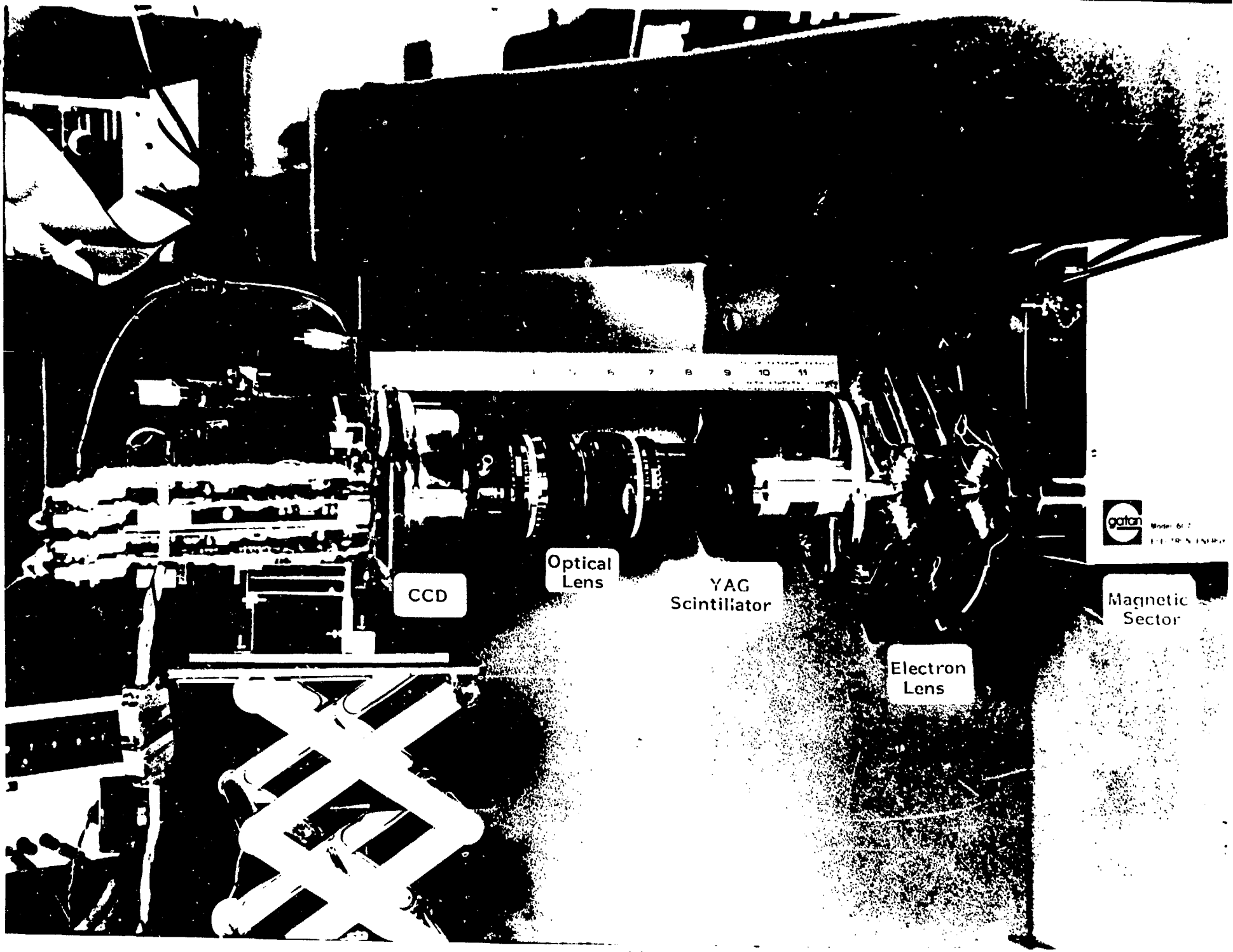
CCD
Optical Lens
YAG Scintillator
Electron Lens
Magnetic Sector
gatan

Fig. 12

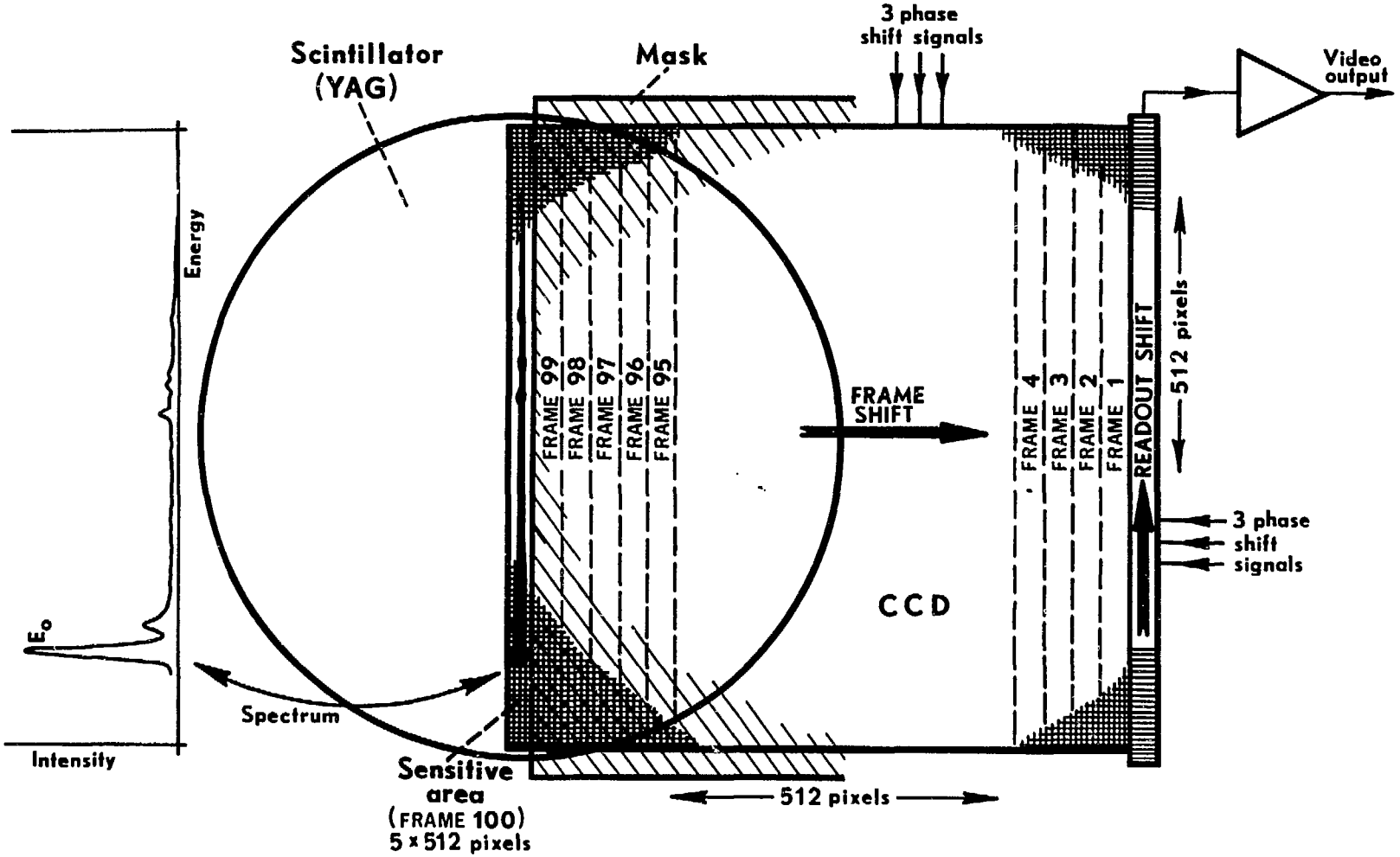
Scintillator
(YAG)
Mask
3 phase
shift signals
Video
output
Energy
E_o
Intensity
Spectrum
FRAME 99
FRAME 98
FRAME 97
FRAME 96
FRAME 95
FRAME
SHIFT
FRAME 4
FRAME 3
FRAME 2
FRAME 1
READOUT SHIFT
512 pixels
3 phase
shift
signals
CCD
Sensitive
area
(FRAME 100)
5 x 512 pixels
512 pixels

Fig. 13

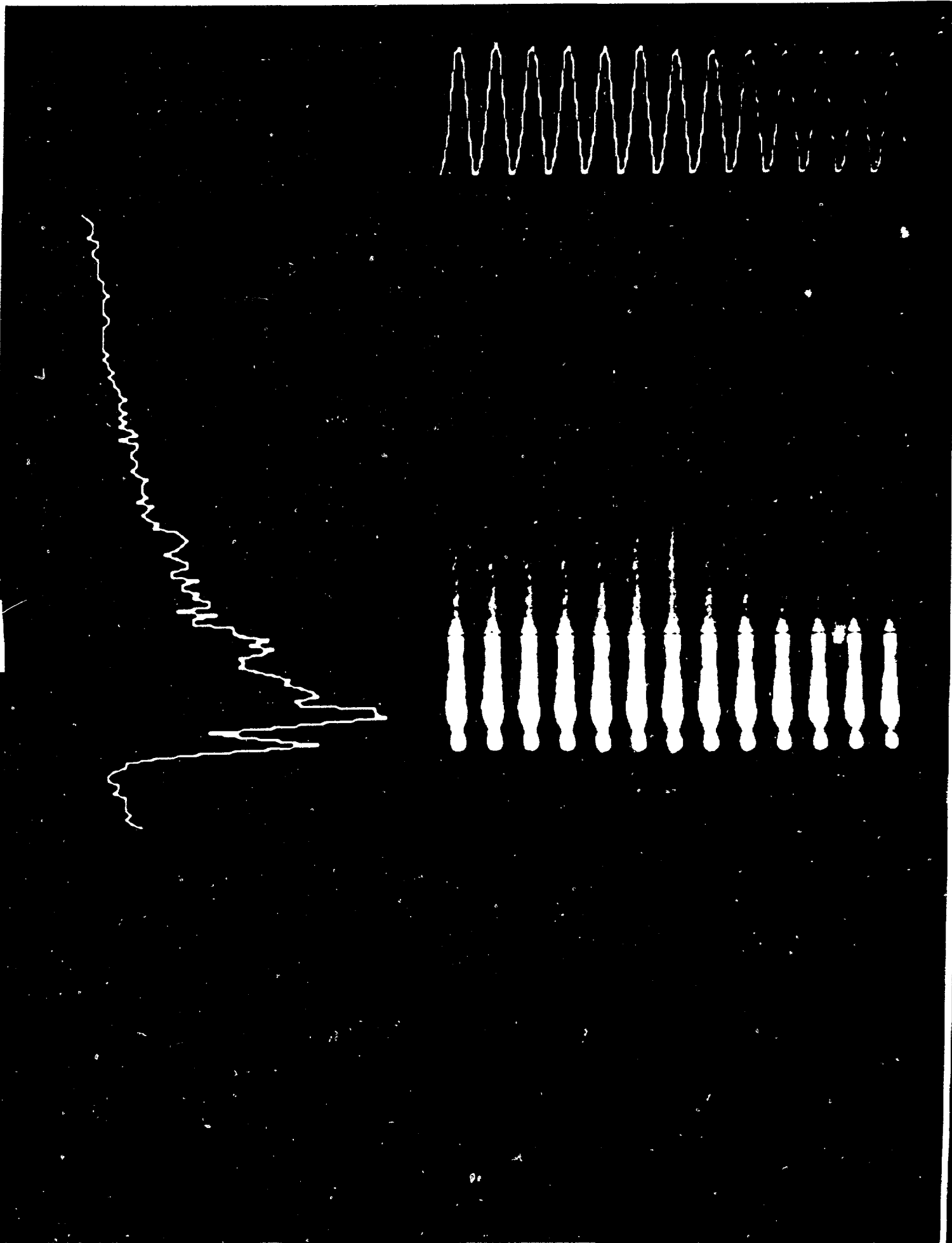

Fig. 14

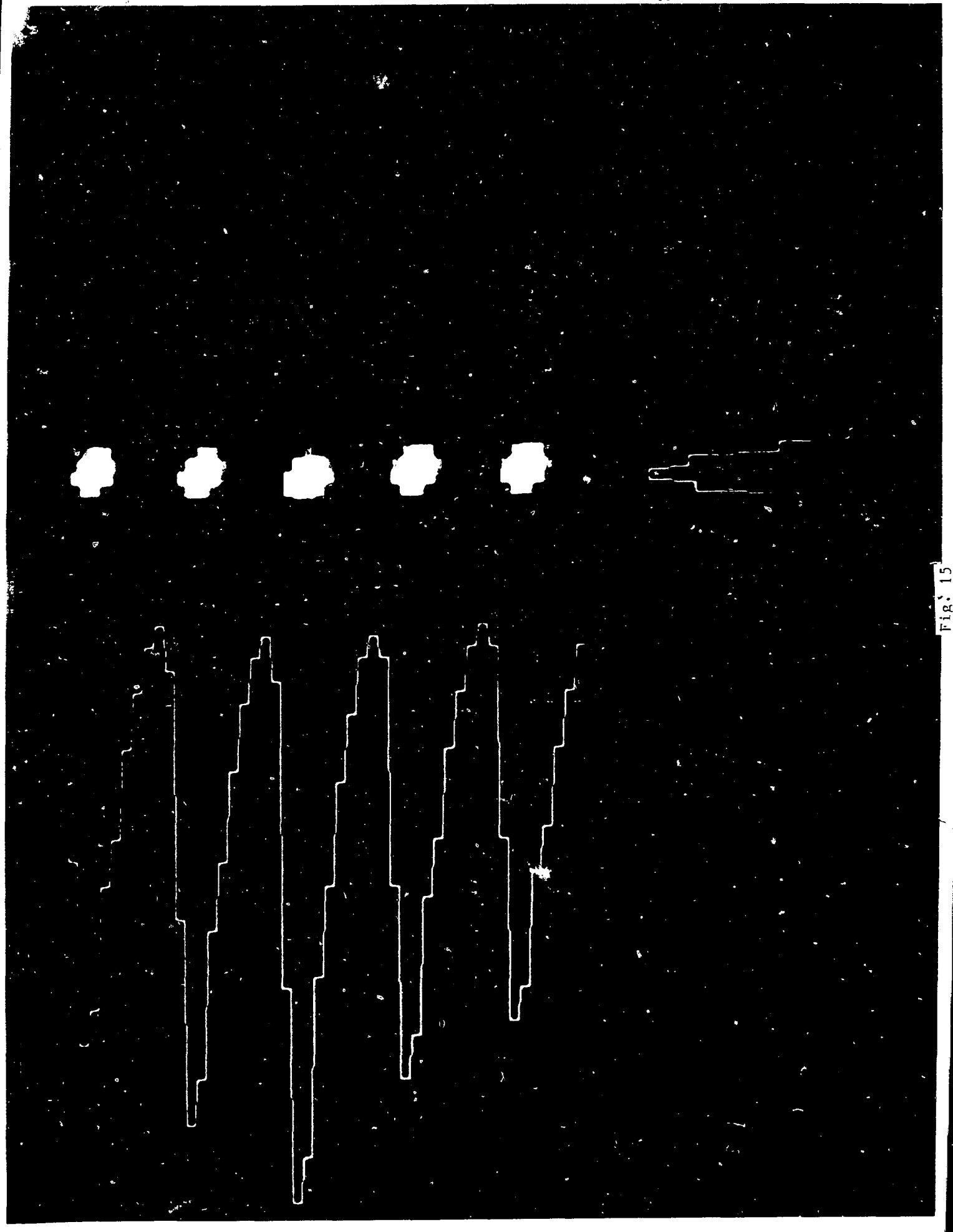

Fig. 15

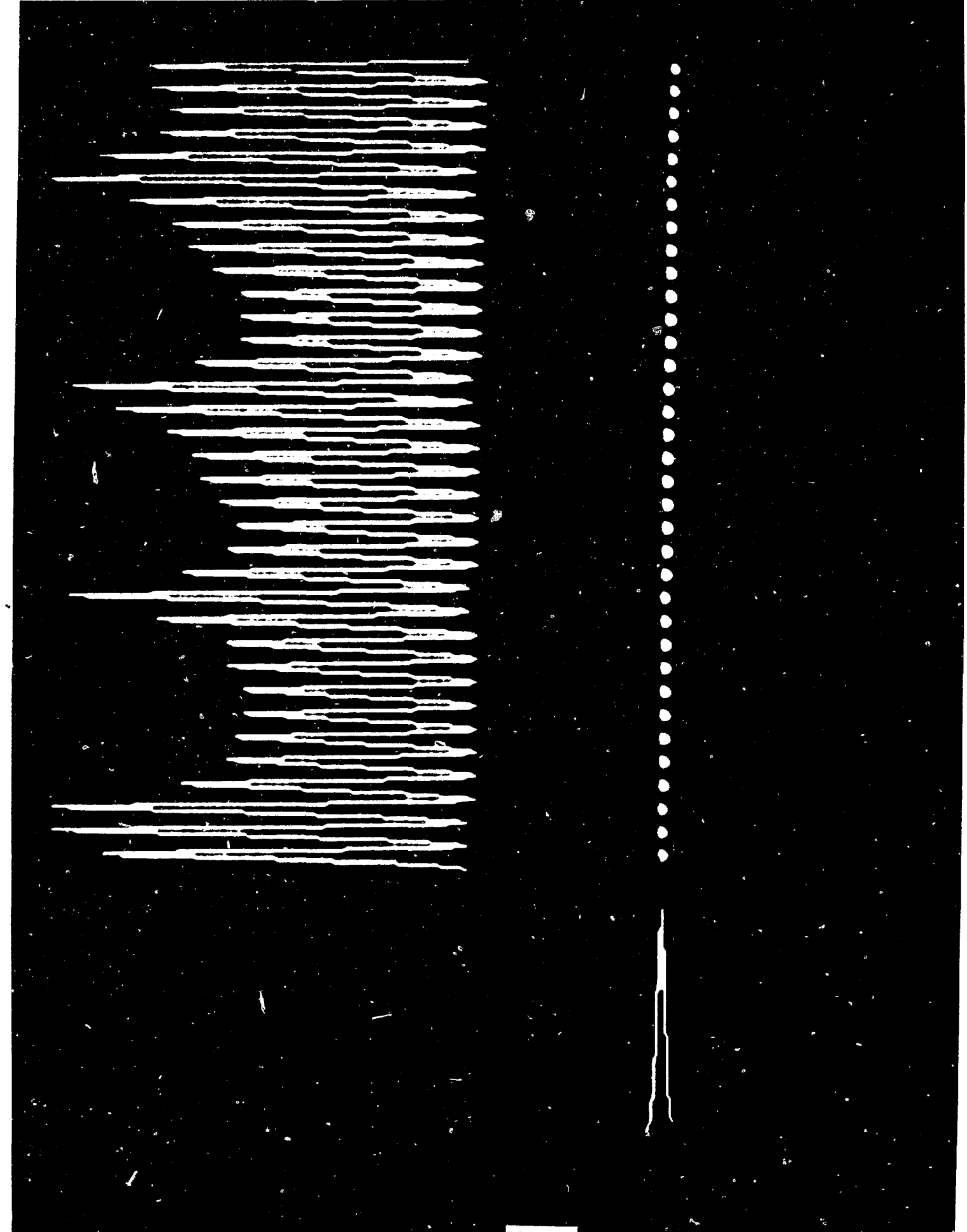

Fig. 16